

ENHANCED RANGE ALIGNMENT USING A COMBINATION OF A POLYNOMIAL AND GAUSSIAN BASIS FUNCTIONS

S. H. Park and H. T. Kim

Department of Electronic & Electrical Engineering,
Pohang University of Science and Technology (POSTECH)
San 31, Hyoja-Dong, Nam-Ku, Pohang, Kyung-buk 790-784, Korea

K. T. Kim

School of Electrical Engineering and Computer Science
Yeungnam University
214-1, Dae-Dong, Gyeongsan-si, Kyungbuk 712-749, Korea

Abstract—For the inverse synthetic aperture radar (ISAR) imaging of a target at a long range, range alignment using the existing polynomial method brings about poor results because the flight trajectory changes depending on the initial position, and the motion parameters, meaning the polynomial cannot fit the trajectory. This paper proposes an improved range alignment method that models the trajectory using a combination of a polynomial and Gaussian basis functions. Initial parameters of the polynomial and Gaussian basis functions are determined by fitting the proposed model to the center of mass curve of the range profile history using the least square curve-fitting algorithm, and the optimum value is found using particle swarm optimization. This method is computationally more efficient and preserves the image quality.

1. INTRODUCTION

Inverse Synthetic Aperture Radar (ISAR) imaging is a technique to generate a high resolution two-dimensional image of a target [1–4]. An ISAR image of the target can be generated by synthesizing many radar signals obtained from various observation angles. Its down-range resolution is directly determined by the bandwidth using Fourier

Corresponding author: K. T. Kim (juniorf@yumail.ac.kr).

transform [5] or time-frequency transform [6]. The radar signal and cross-range are obtained by the Doppler frequency caused by the relative rotational motion between the target and the radar which is generally stationary on the ground. Due to its efficient 2D features, it has been applied for the purpose of automatic target recognition [7–9] along with synthetic aperture radar (SAR) imagery [10, 11].

Among many ISAR imaging techniques, we confine the scope to the range-Doppler algorithm [5]. The key step in this method is the compensation for the translational motion which occurs between pulses in chirp radar systems and bursts in stepped-frequency radars. Without the translational motion compensation, ISAR images can be seriously blurred because reflected signals from the same scatterers can be located at different range bins in different range profiles.

The translational motion compensation is composed of two steps: range alignment and phase adjustment. Range alignment aligns range profiles so that the signals reflected from the same scatterer are placed at the same range bin in different range profiles. Phase adjustment compensates for the Doppler phase errors caused by shifting range profiles in range alignment [12–14].

However, existing range alignment results were mostly obtained when the simulated or the measured targets were at short ranges. In this case, the flight trajectory required for the equal azimuth resolution to the range resolution is relatively short, so the number of range bins is small. Therefore, the alignment is relatively fast, and the polynomials used to model the shifts fit the trajectory well, giving well-aligned range profiles. However, real imaging situations require many range bins because the flight trajectory can be long. In addition, the trajectory is heavily dependent on the initial position and motion parameters. For these reasons, problems such as the computation time arise if the alignment is done using existing methods.

This paper proposes a fast and accurate range alignment method which models the flight trajectory using a combination of a polynomial and Gaussian basis functions. The initial values for the parameters of the polynomial and the Gaussian basis functions are determined by fitting the model to the center of mass (COM) curve of the range profile history using the least square curve-fitting algorithm, which utilizes the gradient descent rule. Then the parameters are optimized using particle swarm optimization (PSO). Simulation results show that the proposed polynomial describes the trajectory accurately and outperforms the conventional methods in terms of the alignment time and image quality.

2. SIGNAL MODEL AND PROPOSED METHOD

2.1. Signal Model and Range-Doppler Algorithm

For the radar signal, we assume a monostatic chirp waveform because it is widely used for high range-resolution. The transmitted chirp signal can be expressed as follows:

$$r(t) = A_0 \exp \left[j2\pi \left(f_0 t + \frac{Bt^2}{2\tau} \right) \right] \text{rect} \left(\frac{t}{\tau} \right) \quad (1)$$

where $r(t)$ is a transmitted signal at time t ; A_0 is the amplitude of the signal; f_0 is the start frequency; B is the bandwidth; τ is the pulse duration; rect is a function whose value is 1 for $t - \tau/2 \leq t \leq t + \tau/2$ and 0 otherwise. Then the received signal reflected from a target composed of K scattering centers is:

$$g(t) = \sum_{k=1}^K A_k \exp \left[j2\pi \left(f_0(t - d_k) + \frac{B(t - d_k)^2}{2\tau} \right) \right] \text{rect} \left(\frac{(t - d_k)}{\tau} \right) \quad (2)$$

where A_k is the amplitude of the k th scattering center, and d_k is the time delay between the radar and k th scattering center. d_k is calculated using the plane wave approximation, in which the distance to a scattering center is projected onto the radar line-of-sight vector. The range-Doppler algorithm compresses the reflected signal using the matched-filter to obtain range profiles at a certain aspect angle. Then, after translational motion compensation by range alignment and phase adjustment, the fast Fourier transform (FFT) is applied to each range bin to resolve scattering centers in the cross-range direction.

2.2. Translational Motion Compensation

Translational motion compensation is composed of two steps: range alignment, which aligns range profiles, and phase adjustment, which removes phase errors caused by the direct shift of each range profile. If a target is stationary and rotating, the signals from the same scatterer will remain in the fixed range bins. However, because targets may travel several range bins between pulses, reflected signals are generally located at different range bins in different range profiles. Therefore, range profiles should be moved so that signals from the same scatterer are placed in the same range bin. In addition, phase errors occur in each range profile if range profiles are aligned without any phase compensation. Thus, these errors should be compensated for.

Popular range alignment methods have utilized the similarity of the envelopes of range profiles using cost functions such as entropy [12]

or correlation [5]. Among several cost functions, 1D entropy is known to be very efficient and robust to noise. It is defined as follows:

$$H_{G_m G_{m+1}} = - \sum_{n=0}^{N-1} \bar{G}(\tau, n) \ln \bar{G}(\tau, n), \quad (3)$$

where $\bar{G}(\tau, n) = \frac{|G_m(n)| + |G_{m+1}(n - \tau)|}{\sum_{n=0}^{N-1} (|G_m(n)| + |G_{m+1}(n - \tau)|)}$

$G_m(n)$ and $G_{m+1}(n)$ are the m th and $(m + 1)$ th range profiles, and N is the total number of range bins. In general, the average of the 1st to m th range profiles is used instead of $G_m(n)$ to minimize the error accumulation in the alignment. According to this criterion, the τ that minimizes the 1D entropy is the shift that best aligns the $(m + 1)$ th range profile.

In addition, efficient methods modeling the range shifts as a polynomial have been proposed to solve the error accumulation problem caused by integer shifts [13, 14]. These methods model the shifts of the range profiles required for the alignment as a polynomial and selects the parameters that maximize the total energy of the sum of aligned range profiles for the alignment.

Phase adjustment uses methods such as the maximum-contrast method and minimum-entropy method [15, 16], which can also be applied even though no information on the motion is given.

2.3. Proposed Range Alignment Method

The range alignment methods mentioned above assume that an imaged target is close to the radar. Therefore, the alignment can be done in a relatively short time because there are not many range bins to search for the minimum of (3). However, when a target is located at a long range, a long flight trajectory is needed to obtain the aspect angle variation required for the cross-range resolution equal to the range resolution. For this reason, much computation time is required to calculate (3) for all range bins; moreover, polynomials proposed to solve error accumulation fail to fit the trajectory because the trajectory is heavily dependent on the initial position and the motion parameters of the target.

In this paper, we model the target trajectory using a combination of a polynomial and Gaussian basis functions as follows. Assuming that there are M range profiles having N range bins, the function that

represents the target trajectory is expressed as

$$P(x) = \sum_{i=0}^L p_i x^i + \sum_{i=0}^G a_i \exp \left[- \left(\frac{x - b_i}{c_i} \right)^2 \right] \quad (4)$$

where $P(x)$ is the trajectory function; $x = 0 \sim M - 1$ with the increment of 1; p_i are parameters for the polynomial; a_i, b_i, c_i are those for the Gaussian basis functions. L is the order of the polynomial, and $G + 1$ is the number of Gaussian functions. The first term of (4) was originally introduced in [13, 14] to model the flight trajectory. However, its main disadvantage is that high-degree fits can become unstable and often fail to fit a trajectory. Therefore, we added the second term to represent the error between the polynomial and the actual flight trajectory. A Gaussian polynomial can be easily implemented, and it was proven that any real function can be expressed by a linear combination of Gaussian basis function [17].

Because N becomes large when the target trajectory is long, the search space to find the parameters in (4) is very wide, and as a result, much time is required when optimization algorithms are used. Therefore, it is very important to set the initial values of the parameters in (4) to save the computation time. In this paper, we initially use the parameters that fit (4) to the center of mass curve of the range profile history. The COM of each range profile is defined as

$$\text{COM}_m = \frac{\sum_{n=0}^{N-1} |G_m(n)| \times n}{\sum_{k=0}^{N-1} |G_m(k)|} \quad (5)$$

where the parameters are the same as in (3). Because values in most range bins are close to zero except for the target regions, the COM is located in the target region. Therefore, we can approximate the trajectory using the COM curve.

The parameters are the least square solution that minimizes the error between the COM data given and the estimated function. Let us assume that the center of mass curve is composed of values $(y_1, y_2, y_3, \dots, y_m)$ for $x = (1, 2, 3, \dots, m)$, and the function to be estimated is $f(x, V)$ calculated by (4), where V is a vector composed of parameters in (4). Then, we find the parameters which minimize the error defined by

$$E = \sum_{i=1}^M e_i^2, \quad \text{where } e_i = y_i - f(x_i, V) \quad (6)$$

The minimum of E is derived when the gradient is zero, that is, for all parameters (elements in V),

$$\frac{\partial E}{\partial V_j} = 2 \sum_{i=1}^M e_i \frac{\partial e_i}{\partial V_j} = 0, \quad (7)$$

where V_j is the j th element of V . Because generally the parameters are not determined in a closed-form, they are calculated in an iterative manner as

$$V_j^{k+1} = V_j^k + \Delta V_j, \quad (8)$$

where ΔV_j is the shift vector which can be derived by the Gauss-Newton algorithm [18] as follows:

$$(J_e^T J_e) \Delta V = -J_e^T e \quad (9)$$

Here, e is a vector of e_i , and J_e is the Jacobian matrix of e with respect to V , which can be calculated by differentiating (6) with respect to each element of V_j . The iteration is performed until E is smaller than a threshold value.

Then, the parameters can be optimized by performing a global optimization algorithm such as a genetic algorithm (GA) [19–25] or PSO. This paper utilizes PSO because it is easier to implement and has been proven to be efficient for several engineering problems [10, 26–31]. PSO is a population based stochastic optimization technique based on the social behavior of bird flocking or fish schooling. The system is initialized with a population of random solutions, called particles, then minimizes the cost function and searches for the optima by changing the velocity of each particle toward the local and the global particle best. The particle dynamics which update each particle is as follows:

$$\vec{v}_i(t) = \phi \vec{v}_i(t-1) + \rho_1(\vec{x}_{pbest} - \vec{x}_i(t)) + \rho_2(\vec{x}_{gbest} - \vec{x}_i(t)), \quad (10)$$

where $\rho_1 = r_1 c_1, \rho_2 = r_2 c_2, r_1, r_2 \approx \text{rand}, c_1, c_2 > 0, c_1 + c_2 < 4$

t is the number of generation, rand is a uniform random number having a uniform distribution between 0 and 1. The velocity vector in the t th generation is then added to the particle $\vec{x}_i(t)$ to move this particle.

After setting several random vectors with elements of the uniform probability distribution between $V \pm \eta V$, where η is a constant smaller than 1, we can utilize the cost function introduced in [14], which represents the energy in the sum of the envelope of the total range profiles, which is defined by

$$E = \sum_{i=1}^N |S(i)|^2, \quad \text{where} \quad S(i) = \sum_{k=1}^M G_k(i) \quad (11)$$

G_k is the k th range profile, and M and N are the number of range profiles and range bins respectively. It can be proven that the shifts that maximize (11) also maximize the contrast of the aligned range profiles. Maximization of the energy can also be achieved by maximizing the following cost function after performing DFT of the envelope of each range profile. (See [14] for the detailed procedure.)

$$E' = \sum_{k=1}^{N/2-1} |S(k)|^2, \quad \text{where} \quad S(k) = \sum_{m=1}^{M-1} A_m(k) \exp\left(-j \frac{2\pi}{N} kn_m\right) \quad (12)$$

A_m is the DFT of the envelope of the m th range profile, and n_m is the shift needed for the m th range profile. N and M are the same as in (11). Once the COM curve is calculated using the parameters optimized, they are rounded to the nearest integers, and each range profile is directly shifted by the number of the corresponding value in the rounded COM curve.

3. EXPERIMENTAL RESULTS

This section presents several examples using targets consisting of point scatterers and a real Boeing 737 aircraft in flight in order to demonstrate the performance of the proposed range alignment algorithm.

3.1. Simulation Results Using a Target of Point Scatterers

A target consisting of 50 isotropic point scatterers was used for the simulation (Fig. 1). To be more realistic, it is modeled using the

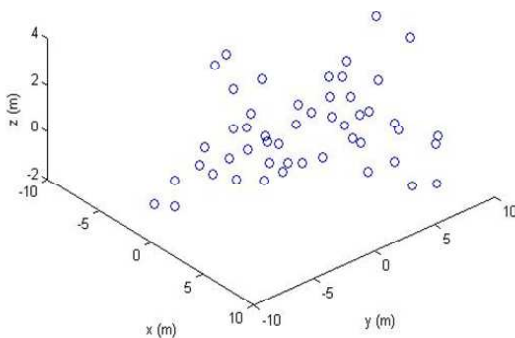


Figure 1. 3D target consisting of 50 point scatterers.

3D CAD data of a real F-14 fighter. The simulation data were obtained by assuming that the target flew from the initial position $[x_0 \ y_0 \ z_0] = [1 \ 100 \ 4]$ km in the $[-1 \ -1 \ 0]$ direction with $v = 280$ m/s and $a = 10$ m/s². The pulse repetition frequency (PRF), center frequency f_0 , bandwidth (BW), and sampling rate associated with the radar system were 2 kHz, 9.15 GHz, 200 MHz (0.75 m range resolution), and 512 MHz respectively. The signal-to-noise ratio (SNR) used was 10 dB. Based on the theory discussed in Section 2, the simulated flight distance required for an equal cross-range resolution was 2.1741 km, and the corresponding number of pulses transmitted at 2 kHz was 31252. For the faster computation, the pulses were down-sampled to 128. Fig. 2 shows the range profiles obtained from the given radar and motion parameters.

The efficiency of the proposed method was demonstrated by comparison with the alignment results of the polynomial method. The polynomial used in [14] is defined as

$$n_m = \sum_{i=1}^{\inf} \beta_i \left(\frac{2m}{M} - 1 \right)^i, \quad 0 \leq m \leq M - 1 \quad (13)$$

where n_m and M are the same as in (12). For each iteration, β_i is increased by a given step size as long as (12) increases with it. When (12) stops increasing (or decreases), the step size is halved, and β_i decreased until it stops increasing. Then the step size is again halved, and the process repeated until the cost function converges. In this step, initial step size is very important because the wrong value can be selected if there are local maxima.

Figure 3 shows the alignment results using n_m derived for each iteration. The initial step size of $N/4$ was used to obtain

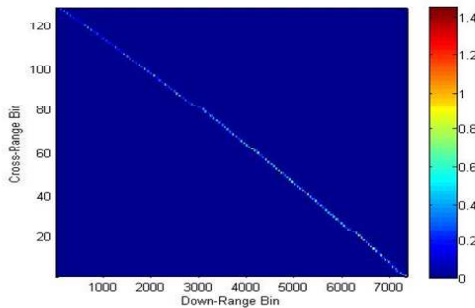


Figure 2. Range profiles for long-range imaging.

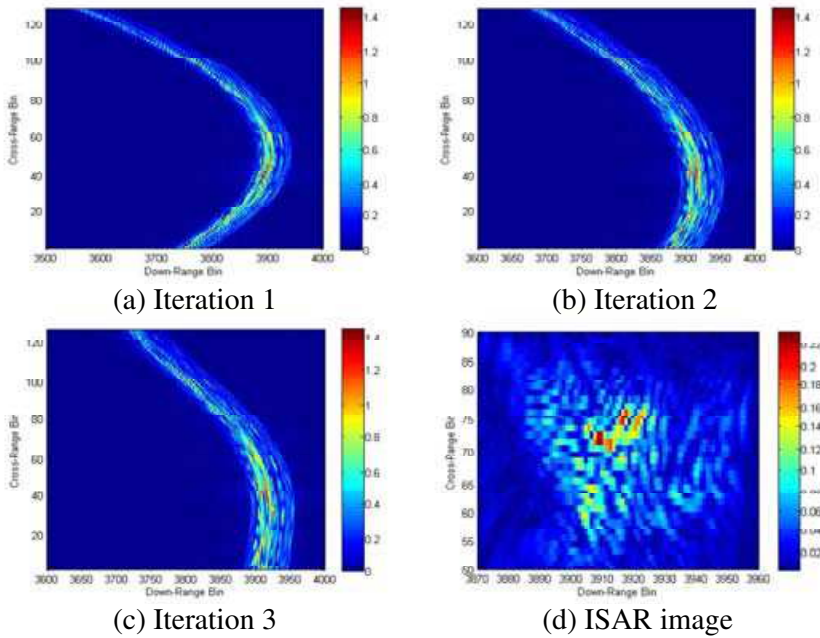


Figure 3. Alignment results using the polynomial method.

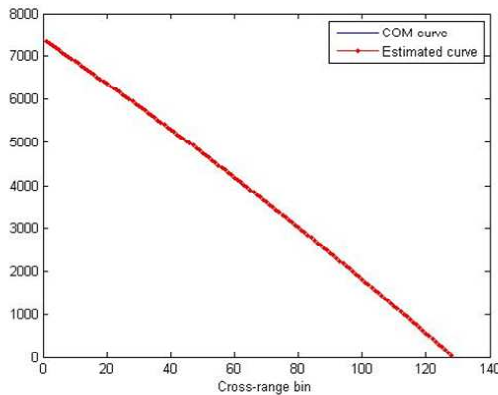


Figure 4. COM curve and estimated curve.

Fig. 3, where N is the number of range bins in each range profile. Even though 8 iterations were carried out, serious alignment errors occurred basically because the polynomial does not represent the flight

trajectory correctly. For this reason, an unrecognizable image was produced.

In contrast, the center of mass curve calculated using (5) and the estimated curve using (6)–(9) closely resemble the flight trajectory in Fig. 2 (Fig. 4). In the estimation of COM curve, L was set to 2, and G was 6. Starting from V with random initial elements between 0 and 1, the program was run until the average difference between the COM curve and the estimated one became smaller than 3. When this condition was not met within 50 iterations, a new V was selected, and the same process was repeated. In optimization, the parameters

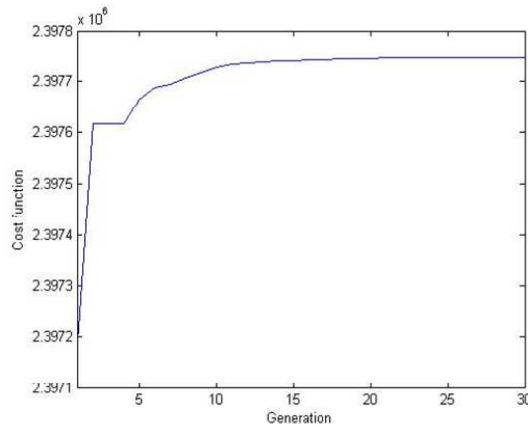


Figure 5. Evolution curve.

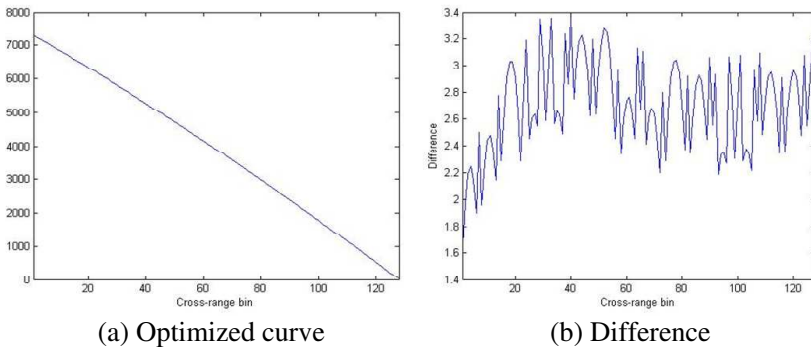


Figure 6. Optimized curve and the difference between the optimized curve and the COM curve.

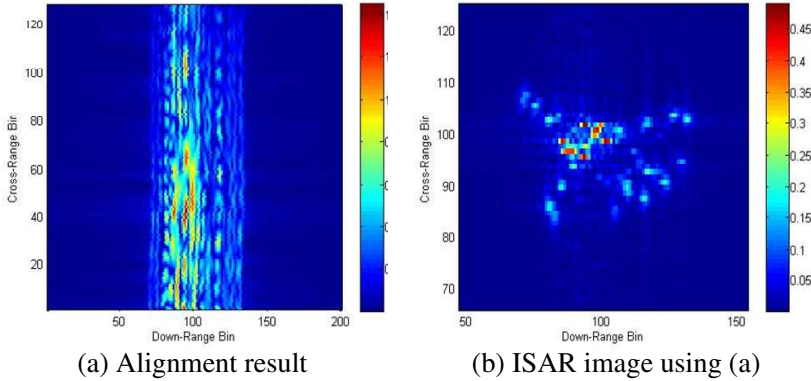


Figure 7. Range alignment result and ISAR image derived using the proposed method

Table 1. Comparison of alignment results for each method (point scatterers).

Method	Energy of sum envelope	Entropy of ISAR images	Computation time (sec)
Polynomial	55867.634	7.651	265.205
Proposed method	122095.324	5.756	25.705

used in PSO were population size = 20, number of generations = 30, $\phi = 0.5$, and $c_1 = c_2 = 1.49$. Each particle was initialized in the range of $V \pm \eta V$, where $\eta = 0.0005$. Because the parameters estimating the COM curve represented the trajectory approximately, the evolution curve converged within 30 generations (Fig. 5), yielding the optimized trajectory, whose values were different by less than 3.5 (Figs. 6(a) and (b)). As a result, the alignment result and the focused ISAR image are much better than the alignment using (6) (Figs. 7(a) and (b)).

Table 1 quantifies the performance in terms of the energy in the sum envelope of the range profiles aligned, entropy of the image after phase adjustment, and the computation time for the alignment. The program was written in Matlab R2007a and run in Windows XP on an Intel Quadcore processor. The entropy of the image was calculated by

$$Ent = \sum_{i=1}^M \sum_{j=1}^N |I(i, j)|^2 \ln |I(i, j)|^2 \tag{14}$$

where $I(i, j)$ is the (i, j) th pixel value of the ISAR image.

As we can see, the alignment using the polynomial in (13) gives a poor result because of the mismatch (Fig. 3). Even though the entropy of the ISAR image is very low, the image does not show a recognizable target due to the poor alignment. In addition, the computation time was more than 4 minutes because the cost function used seldom converged. Clearly, the proposed method needs a much less time (25.705 s) than the existing method and produces a well-focused image at the same time. The computation time can be further reduced if COM curve is constructed in (5), and the proposed procedure is carried out using a downsampled image, such as $M/4$ by N .

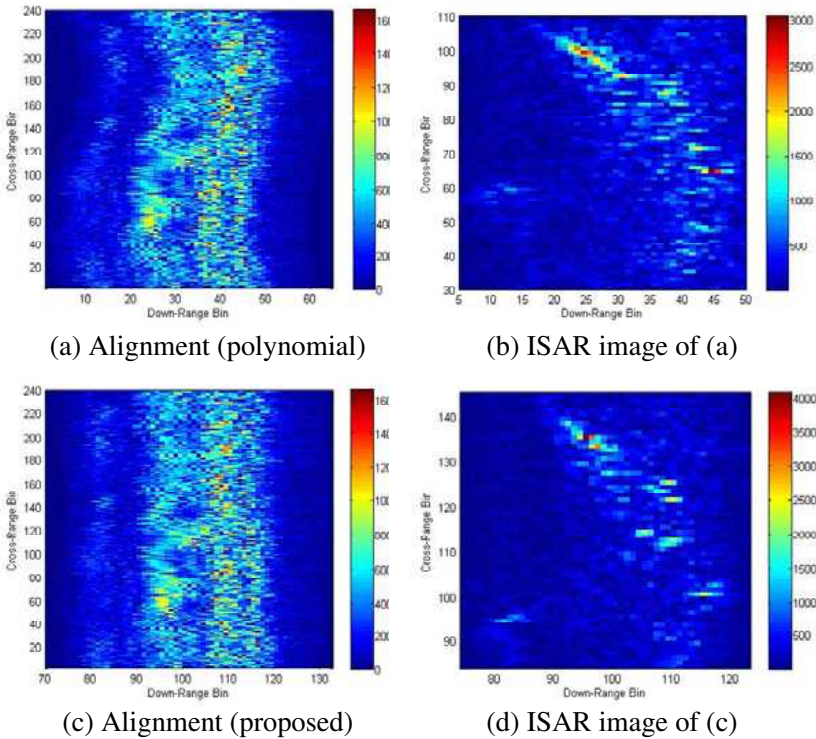


Figure 8. Comparison of alignment results between the polynomial method and the proposed method.

Table 2. Comparison of alignment results for each method (Boeing 737).

Method	Energy of sum envelope	Entropy of ISAR images	Computation time (sec)
Polynomial	$3.567e + 013$	6.998	192.898
Proposed method	$3.801e + 013$	6.012	20.87

3.2. Simulation Results Using the Measured Data from a Boeing 737 Aircraft

The proposed method was applied to the real ISAR data derived from a Boeing 737 aircraft taking off at 3 km distance. Because the distance to the target is very short, range profiles are located in a close range. To simulate range alignment for long-range ISAR imaging, each range profile after the proposed alignment was shifted following a polynomial modeled by

$$\text{Poly} = -5x^2/M + 20x + 1, \quad x = -M/2 \sim M/2 - 1 \quad (15)$$

where M is the number of the range profiles.

Figure 8 shows the alignment results for each method and the corresponding ISAR images, and Table 2 quantifies their performance. The same parameters as in the point scatterer case were used. Range profiles using the polynomial in Fig. 8(a) are curved, yielding the poorest ISAR image in (b). However, the results in (c) and (d) and Table 2 prove that the proposed method consumes less time and preserves the accuracy.

4. CONCLUSION

The proposed three-step range alignment method effectively aligns range profiles for long-range ISAR imaging, for which the flight trajectory is not represented by a single polynomial. It reduces the computation time and preserves the accuracy in alignment. The first step is to model the trajectory using a combination of a polynomial and Gaussian basis functions and to find their parameters using the least square curve-fitting algorithm. This significantly reduces the convergence speed of the cost function by narrowing down the search space. The second step is to find the optimum parameters that maximize the energy of the sum envelope of range profiles. Simulation results using a target composed of point scatterers and measured data of a Boeing 737 prove that the proposed method is more efficient than the polynomial-only method.

ACKNOWLEDGMENT

This research was supported by the Yeungnam University research grants in 2008.

REFERENCES

1. Chen, C. C. and H. C. Andrews, "Target-motion-induced radar imaging," *IEEE Trans. Aerospace and Electronic Systems*, Vol. 16, No. 1, 2–14, Jan. 1980.
2. Park, S.-H., K.-K. Park, J.-H. Jung, H.-T. Kim, and K.-T. Kim, "ISAR imaging of multiple targets using edge detection and Hough transform," *Journal of Electromagnetic Waves and Applications*, Vol. 22, No. 2–3, 365–373, 2008.
3. Park, S.-H., K.-K. Park, J.-H. Jung, H.-T. Kim, and K.-T. Kim, "Construction of training database based on high frequency RCS prediction methods for ATR," *Journal of Electromagnetic Waves and Applications*, Vol. 22, No. 5–6, 693–703, 2008.
4. Ma, C. Z., T. S. Yeo, H. S. Tan, and G. Lu, "Interferometric ISAR imaging on squint model," *Progress In Electromagnetics Research Letters*, Vol. 2, 125–133, 2008.
5. Ausherman, D. A., A. Kozma, J. L. Walker, H. M. Jones, and E. C. Poggio, "Development in radar imaging," *IEEE Trans. Aerosp. Electron. Syst.*, Vol. 20, No. 4, 363–400, Jul. 1984.
6. Xue, W. and X.-W. Sun, "Target detection of vehicle volume detecting radar based on Wigner-Hough transform," *Journal of Electromagnetic Waves and Applications*, Vol. 21, No. 11, 1513–1523, 2007.
7. Menon, M. M., E. R. Boureau, and P. J. Kolodzy, "An automatic ship classification system for ISAR imagery," *The MIT Lincoln Laboratory Journal*, Vol. 6, No. 2, 289–308, 1993.
8. Jung, J.-H. and H.-T. Kim, "Comparison of four feature extraction approaches based on Fisher's linear discriminant criterion in radar target recognition," *Journal of Electromagnetic Waves and Applications*, Vol. 21, No. 2, 251–265, 2007.
9. Lee, K. C. and J. S. Ou, "Radar target recognition by using linear discriminant algorithm on angular-diversity RCS," *Journal of Electromagnetic Waves and Applications*, Vol. 21, No. 14, 2033–2048, 2007.
10. Lim, T. S., V. C. Koo, H.-T. Ewe, and H.-T. Chuah, "A SAR autofocus algorithm based on particle swarm optimization," *Progress In Electromagnetics Research B*, Vol. 1, 159–176, 2008.

11. Lim, T. S., C.-S. Lim, V. C. Koo, H.-T. Ewe, and H.-T. Chuah, "Autofocus algorithms performance evaluations using an integrated SAR product simulator and processor," *Progress In Electromagnetics Research B*, Vol. 3, 315–329, 2008.
12. Li, X., G. Liu, and J. Ni, "Autofocusing of ISAR images based on entropy minimization," *IEEE Trans. Aerosp. Electron. Syst.*, Vol. 35, No. 4, 1240–1251, Oct. 1999.
13. Wang, J. and D. Kasilingam, "Global range alignment for ISAR," *IEEE Trans. Aerosp. Electron. Syst.*, Vol. 39, No. 1, 351–357, Jan. 2003.
14. Wang, J. and X. Liu, "Improved global range alignment for ISAR," *IEEE Trans. Aerosp. Electron. Syst.*, Vol. 43, No. 3, 1070–1075, Jul. 2007.
15. Berizzi, F. and G. Cosini, "Autofocusing of inverse synthetic radar images using contrast optimization," *IEEE Trans. Aerosp. Electron. Syst.*, Vol. 32, No. 3, 1191–1197, Jul. 1996.
16. Wang, J., X. Liu, and Z. Zhou, "Minimum-entropy phase adjustment for ISAR," *Proceedings of Radar, Sonar and Navigation*, Vol. 151, No. 4, 203–209, Aug. 2004.
17. Qian, S. and D. Chen, "Signal representation using adaptive normalized Gaussian functions," *Signal Processing*, Vol. 36, No. 1, 1–11, Mar. 1994.
18. George, A., F. Seber, and C. J. Wild, *Nonlinear Regression*, Wiley-Interscience, 2003.
19. Su, D. Y., D.-M. Fu, and D. Yu, "Genetic algorithms and method of moments for the design of PIFAS," *Progress In Electromagnetics Research Letters*, Vol. 1, 9–18, 2008.
20. Razavi, S. M. J. and M. Khalaj-Amirhosseini, "Optimization an anechoic chamber with ray-tracing and genetic algorithms," *Progress In Electromagnetics Research B*, Vol. 9, 53–68, 2008.
21. Liu, B., L. Beghou, L. Pichon, and F. Costa, "Adaptive genetic algorithm based source identification with near-field scanning method," *Progress In Electromagnetics Research B*, Vol. 9, 215–230, 2008.
22. Chen, H.-T., G.-Q. Zhu, and S.-Y. He, "Using genetic algorithm to reduce the radar cross section of three-dimensional anisotropic impedance object," *Progress In Electromagnetics Research B*, Vol. 9, 231–248, 2008.
23. Ngo Nyobe, E. and E. Pemha, "Shape optimization using genetic algorithms and laser beam propagation for the determination of the diffusion coefficient in a hot turbulent jet of air," *Progress In*

- Electromagnetics Research B*, Vol. 4, 211–221, 2008.
24. Cengiz, Y. and H. Tokat, “Linear antenna array design with use of genetic, memetic and tabu search optimization algorithms,” *Progress In Electromagnetics Research C*, Vol. 1, 63–72, 2008.
 25. Rostami, A. and A. Yazdanpanah-Goharrizi, “Hybridization of neural networks and genetic algorithms for identification of complex bragg gratings,” *Journal of Electromagnetic Waves and Applications*, Vol. 22, No. 5–6, 643–664, 2008.
 26. Hassan, R., B. Cohanım, and O. Weck, “A comparison of particle swarm optimization and the genetic algorithm,” *46th AIAA/ASME/ASCE/AHS/ASC Structures, Structural Dynamics & Materials Conference*, Apr. 18–21, 2005.
 27. Li, J.-F., B.-H. Sun, Q.-Z. Liu, and L. Gong, “PSO-based fast optimization algorithm for broadband array antenna by using the cubic spline interpolation,” *Progress In Electromagnetics Research Letters*, Vol. 4, 173–181, 2008.
 28. Panduro, M. A., C. A. Brizuela, L. I. Balderas, and D. A. Acosta, “A comparison of genetic algorithms, particle swarm optimization and the differential evolution method for the design of scannable circular antenna arrays,” *Progress In Electromagnetics Research B*, Vol. 13, 171–186, 2009.
 29. Lu, Z. B., A. Zhang, and X. Y. Hou, “Pattern synthesis of cylindrical conformal array by the modified particle swarm optimization algorithm,” *Progress In Electromagnetics Research*, PIER 79, 415–426, 2008.
 30. Liu, X. F., Y. C. Jiao, and F. S. Zhang, “Conformal array antenna design using modified particle swarm optimization,” *Journal of Electromagnetic Waves and Applications*, Vol. 22, No. 2–3, 207–218, 2008.
 31. Park, S.-H., H.-T. Kim, and K.-T. Kim, “Stepped-frequency ISAR motion compensation using particle swarm optimization with an island model,” *Progress In Electromagnetics Research*, PIER 85, 25–37, 2008.